materials

MDPI

Article

Investigation of Mechanical and Microstructural Properties of Welded Specimens of AA6061-T6 Alloy with Friction Stir Welding and Parallel-Friction Stir Welding Methods

Amir Ghiasvand [1], Mohammad Mahdi Yavari [2], Jacek Tomków [3], John William Grimaldo Guerrero [4], Hasan Kheradmandan [5], Aleskei Dorofeev [6], Shabbir Memon [7] and Hesamoddin Aghajani Derazkola [8,*]

[1] Department of Mechanical Engineering, University of Tabriz, Tabriz 5166616471, Iran; Amir.ghiasvand@tabrizu.ac.ir
[2] Department of Mechanical Engineering, Kermanshah Branch, Islamic Azad University, Kermanshah 67189-97551, Iran; Mmahdiyavarisep@gmail.com
[3] Institute of Machines and Materials Technology, Faculty of Mechanical Engineering and Ship Technology, Gdańsk University of Technology, Gabriela Narutowicza Street 11/12, 80-233 Gdańsk, Poland; jacek.tomkow@pg.edu.pl
[4] Departamento de Energía, Univesidad de la Costa, Barranquilla 55-66, Colombia; jgrimald1@cuc.edu.co
[5] Department of Mechanical Engineering, Arak Branch, Islamic Azad University, Arak 38361-1-9131, Iran; kheradmandan.hasan@gmail.com
[6] Department of Propaedeutics of Dental Diseases, Sechenov First Moscow State Medical University, 119991 Moscow, Russia; sfmsmu@mail.ru
[7] Department of Mechanical Engineering, Wichita State University, Wichita, KS 67260-133, USA; sxmemon@shockers.wichita.edu
[8] Department of Mechanical Engineering, Islamic Azad University of Nour Branch, Nour 21655432, Iran
* Correspondence: h.aghajany@live.com

Citation: Ghiasvand, A.; Yavari, M.M.; Tomków, J.; Guerrero, J.W.G.; Kheradmandan, H.; Dorofeev, A.; Memon, S.; Derazkola, H.A. Investigation of Mechanical and Microstructural Properties of Welded Specimens of AA6061-T6 Alloy with Friction Stir Welding and Parallel-Friction Stir Welding Methods. *Materials* **2021**, *14*, 6003. https://doi.org/10.3390/ma14206003

Academic Editors: Eduardo Garcia, Alberto Murillo-Marrodán, Hamed Aghajani Derazkola and Tomasz Trzepieciński

Received: 7 September 2021
Accepted: 11 October 2021
Published: 12 October 2021

Publisher's Note: MDPI stays neutral with regard to jurisdictional claims in published maps and institutional affiliations.

Abstract: The present study investigates the effect of two parameters of process type and tool offset on tensile, microhardness, and microstructure properties of AA6061-T6 aluminum alloy joints. Three methods of Friction Stir Welding (FSW), Advancing Parallel-Friction Stir Welding (AP-FSW), and Retreating Parallel-Friction Stir Welding (RP-FSW) were used. In addition, four modes of 0.5, 1, 1.5, and 2 mm of tool offset were used in two welding passes in AP-FSW and RP-FSW processes. Based on the results, it was found that the mechanical properties of welded specimens with AP-FSW and RP-FSW techniques experience significant increments compared to FSW specimens. The best mechanical and microstructural properties were observed in the samples welded by RP-FSW, AP-FSW, and FSW methods, respectively. Welded specimens with the RP-FSW technique had better mechanical properties than other specimens due to the concentration of material flow in the weld nugget and proper microstructure refinement. In both AP-FSW and RP-FSW processes, by increasing the tool offset to 1.5 mm, joint efficiency increased significantly. The highest weld strength was found for welded specimens by RP-FSW and AP-FSW processes with a 1.5 mm tool offset. The peak sample of the RP-FSW process (1.5 mm offset) had the closest mechanical properties to the base metal, in which the Yield Stress (YS), ultimate tensile strength (UTS), and elongation percentage (E%) were 76.4%, 86.5%, and 70% of base metal, respectively. In the welding area, RP-FSW specimens had smaller average grain size and higher hardness values than AP-FSW specimens.

Keywords: parallel-friction stir welding; tool offset; mechanical properties; aluminum alloy

1. Introduction

Among solid-state joining techniques, Friction Stir Welding (FSW) is a relatively new and useful technique used in various industries such as aerospace, marine, and automotive industries [1–4]. In the FSW process, a non-consumable rotating tool heats the two pieces due to the contact and intense friction between the two pieces [5–7]. Many factors

affect the FSW joint, which are classified into two general categories of process parameters and tool geometry [5–7]. By changing the condition of each of the parameters, the heat and material flow distribution in the process change, which ultimately leads to a change in the mechanical quality of the joint [8–13]. The most important factors influencing the FSW process are the temperature and the material flow distribution patterns in the welding zone [14–18]. The heat and flow of materials created in the process derive from two factors: welding geometry and tool geometry. In the FSW process, two different zones are formed on either side of the weld line [19–23]. The side where the tool pin surface rotation direction and the tool traverse direction have the same vectorial sense is called the Advancing Side (AS), and the side where the tool pin surface rotation direction and the tool traverse direction have the opposite vectorial sense is called the Retreating Side (RS) [11,16,17]. The two regions of the AS and RS have significant differences in the way of heat distribution and plastic flow patterns, which cause significant differences in mechanical and metallurgical quality in these areas [24]. The most important disadvantage of the linear FSW process is the lack of symmetry on either side of the weld [25–28]. If the asymmetry in the temperature distribution and material flow in the FSW process can be eliminated and the process turns into a relatively symmetrical process, the mechanical quality of the joint can be improved [29–31]. Different solutions have been suggested to eliminate this disadvantage, which includes the use of Reverse Dual-Rotation Friction Stir Welding (RDR-FSW) [32,33], implementation of the FSW process using tandem tools, using Multi-Pass Friction Welding (MP- FSW) [34–36] with reverse rotation of the tool and the use of Parallel-Friction Stir Welding (P-FSW) [37].

A few pieces of research have been performed in the mentioned fields. Li et al. [32,33] investigated the RDR-FSW of AA2019-T6 aluminum alloy. Based on their findings, it was found that the use of the aforesaid technique significantly increases the mechanical and metallurgical quality of the joint and reduces the required force and torsional torque to perform the process. Shi et al. [38] modeled the RDR-FSW process thermo-mechanically. Based on the results, it was found that the use of the RDR-FSW technique leads to relative symmetry in heat distribution and plastic flow. In this method, two tools move in a line with reverse rotational speeds and perform the welding process. According to their results, this method has significant advantages over the conventional FSW process, such as reducing clamping force, torsional torque, and process defects and increasing joint efficiency. Liu and Zhang [39] used the re-welding of the weld line technique to eliminate the groove defects. In the second pass, they reversed the tool rotation sense. Based on the results, it was found that the use of this method eliminates defects and significantly increases joint efficiency. Kumari et al. [40] investigated the two-pass FSW process by reversing the direction of tool rotation in the first and second passes. According to the reported results, the use of the MP-FSW technique with reverse rotation caused a significant increase in the mechanical properties of the joint. Jain et al. [41] investigated and numerically simulated the FSW process of inverted inline twin-pin tools with inverted rotation directions. It was found that the use of this tool increases the peak process temperature and symmetry of the strain distribution and strain rate in the process and reduces the defects of the FSW process. Ghiasvand et al. [42] introduced a new two-pass FSW method called P-FSW for welding two dissimilar aluminum alloys AA6061-T6 and AA7075-T6. Welding was performed in two passes with the same welding directions and different rotations of the tool, and in each pass, different offsets were used for the tool. Based on the obtained results, it was found that in case of using optimal values of tool offsets in the first and second passes, the joint efficiency for dissimilar welding sample increases significantly.

Due to the fact that no research has been performed in the field of P-FSW technique other than the one mentioned above, the need for further studies in this field seems to be necessary. In the welding process of dissimilar materials with this method, the offset of the tool in the first and second passes and the type of P-FSW process are determined based on the difference in mechanical properties of the two materials participating in the joint.

However, in the welding of similar parts with the P-FSW technique same offsets in both passes must be used. Therefore, in the present study, the effects of two parameters of the tool offset and type of process on the mechanical, microhardness, and microstructure properties of FSW and P-FSW of AA6061-T6 alloy joints have been investigated.

2. Materials and Methods

2.1. Welding Methods

In the present study, the convectional FSW method and the new P-FSW method have been used for welding. In the P-FSW method, welding is performed in two passes with the same welding direction and different tool rotation directions. For welding similar parts with this method, the first and second welding passes are performed symmetrically and with the same offsets. The directions of rotation of the tool are reverse in two passes to create relative symmetry in the temperature distribution and plastic flow created in the workpiece. According to the direction of rotation of tools in welding passes, this process has two different types [42]. If the direction of the tool rotation in the first and second passes of welding is such that the marginal zones of the welding line are in the RS region and the weld line is entirely in the AS region, the Advancing Parallel-Friction Stir Welding (AP-FSW) is formed and in reverse conditions of the mentioned condition, i.e., when the marginal zones of the weld line are in the AS region and the weld line is in the RS region, the Retreating Parallel-Friction Stir Welding (RP-FSW) is formed. The schematic of the FSW process and the two processes of RP-FSW and AP-FSW have been shown in Figure 1.

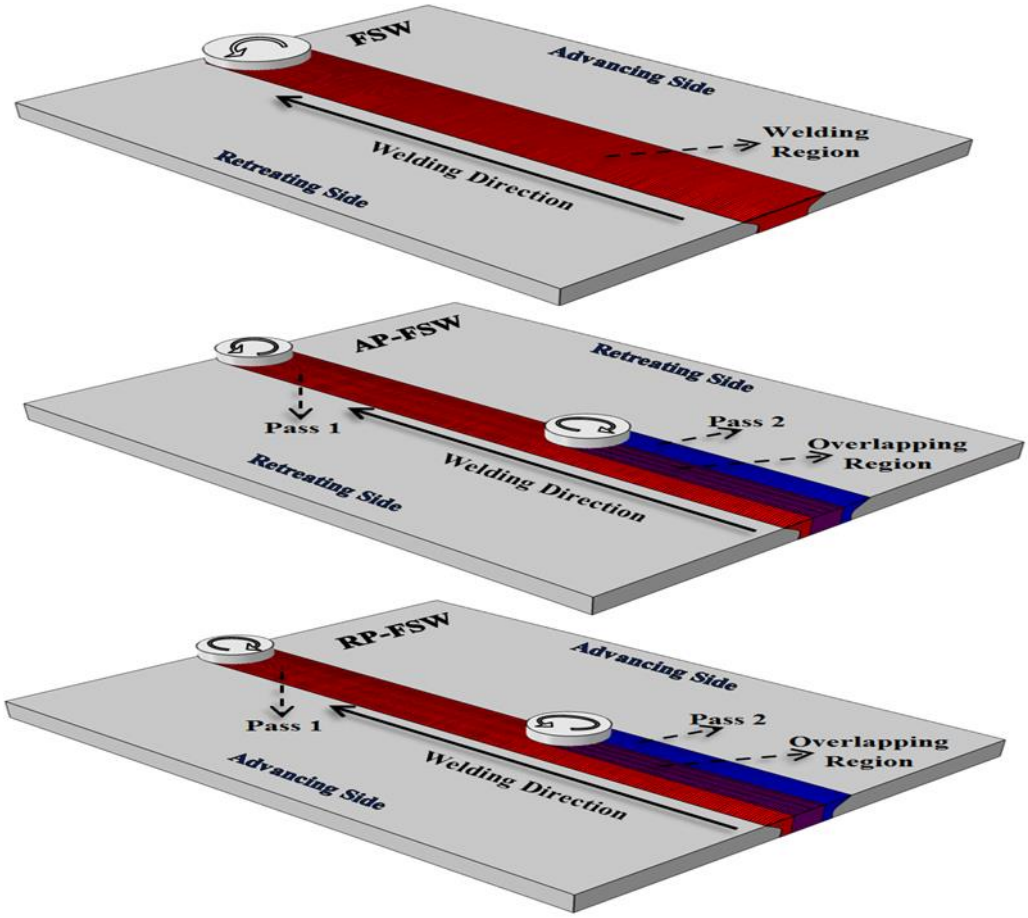

Figure 1. The schematic of the FSW, RP-FSW, and AP-FSW processes.

2.2. Workpiece, Tool, and Welding Machine

AA6061-T6 aluminum alloy, which is widely used in aerospace, marine, and automotive industries, was used to perform three techniques: FSW, AP-FSW, and RP-FSW. The chemical composition and mechanical properties of AA6061-T6 alloy have been shown in Tables 1 and 2, respectively. The chemical composition was performed by emission spectroscopy (Hitachi, Japan) according to the ASTM E415 number.

Table 1. Chemical composition of AA6061-T6 alloy.

Chemical Composition (%)								
Al	Mg	Si	Cu	Fe	Cr	Mn	Zn	Ti
Balance	0.81	0.61	0.29	0.2	0.13	0.03	0.02	0.01

Table 2. Mechanical properties of AA6061-T6 alloy.

Yield Stress (MPa)	Ultimate Tensile Strength (MPa)	Elongation (%)
268	330	17

Weld geometry was considered as butt weld, and the dimensions of the parts participating in the joint in all samples were considered equal to 120 mm × 50 mm × 5 mm. Before starting the welding, the surfaces of the samples were polished with sandpaper of different grades and cleaned using acetone to reduce the possibility of impurities. As mentioned, the FSW process was performed in one welding pass, and the two processes AP-FSW and RP-FSW were performed in two welding passes. For samples welded by AP-FSW and RP-FSW methods, the first and second passes were performed in the same directions, and in each pass, the direction of tool rotation and tool position were reversed from the weld line. It should be noted that in all samples welded by AP-FSW and RP-FSW methods, the second welding pass was performed as soon as the first pass was completed. The convectional milling machine was used for welding. In order to fix the workpieces during the welding process, a suitable fixture was designed, and the workpiece was placed on the milling machine table during the welding process. The welding machine and fixture are shown in Figure 2.

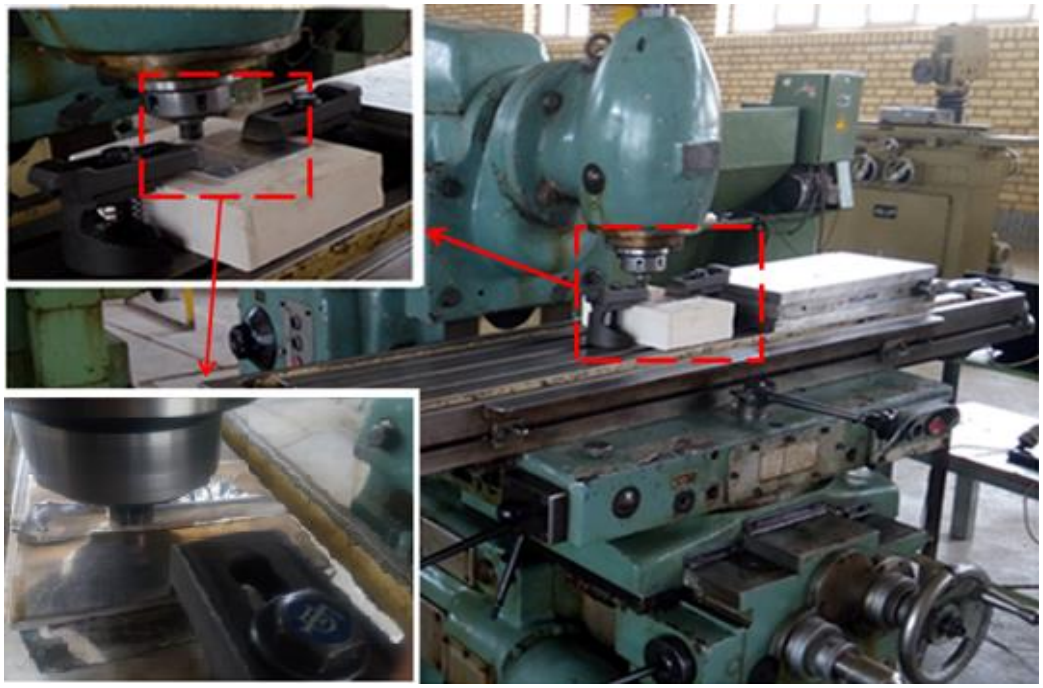

Figure 2. Schematic of milling machine and workpiece.

In the FSW-based process, tools must be such that their functions are kept at high temperatures, and their mechanical properties do not change [43–45]. Therefore, H13 steel, which is a versatile chromium-molybdenum hot work steel that is widely used in hot work and cold work tooling applications, was used to make all the tools used, and after that, thermal hardening operations were performed on the tools to increase their hardness [46]. To perform three welding processes, a tool was used that its shoulder diameter, pin diameter, and pin length were 20, 5, and 4.7 mm, respectively. The tool used in the FSW and P-FSW processes has been shown in Figure 3. The shoulder depth in all welding specimens was 0.1 mm. The dwell time for the first welding pass of all the samples was the same (5 s).

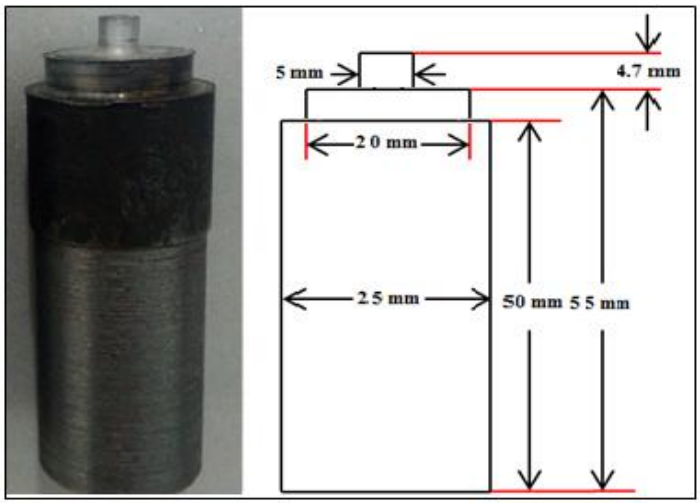

Figure 3. The tool used in FSW and P-FSW processes.

2.3. Welding Parameters and Experimental Models

Due to the fact that the process parameters (traveling speed and rotational speed of the tool) play an influential role in the mechanical quality and microstructure of the welded parts, these parameters must be set at their optimal condition. For this purpose, in accordance with the proposed values in the literature review [47], the traveling and the rotational speed were set equal to 60 mm/min and 1180 rpm, respectively. In addition, the tilt angle was equal to 2 degrees. It should be noted that the same process parameters were used for all welding samples.

As mentioned, in this study, the effects of two parameters of the type of welding process and tool offset on the mechanical and microstructural properties of the joint are investigated. Three welding processes, FSW, AP-FSW, and RPSW, have been used to investigate the effect of the type of welding process. In addition, in order to investigate the tool offset impact, 4 different offset values of 0.5, 1, 1.5, and 2 mm were used in two welding passes in two P-FSW processes, AP-FSW and RP-FSW. It should be noted that the tool offsets in both welding passes were equal and in reverse directions. A total of nine welding samples were performed, which differed in the type of welding process and the value of the tool offsets. The input parameters and their values of the nine experimental models have been shown in Table 3.

Table 3. Experimental models.

Model's Name	Process Type	Tool Offset (mm)
Base	FSW	0
A0	AP-FSW	0.5
A0.5		1
A1		1.5
A2		2
R0.5	RP-FSW	0.5
R1		1
R1.5		1.5
R2		2

2.4. Mechanical and Metallographic Tests

Vickers hardness test and tensile test were used to investigate the effect of the mentioned parameters on the welding joint. The SANTAM STM-25KN tensile test apparatus (Tehran, Iran) was used to perform the tensile test. Samples were cut perpendicular to the weld line. The samples were prepared according to the ASTM-E8M standard [48,49]. It should be noted that three tensile test samples were prepared from each welded specimen, and the results are based on the average of the three specimens. The schematic of the tensile test specimen and the cutting position of three tensile tests have been shown in Figure 4.

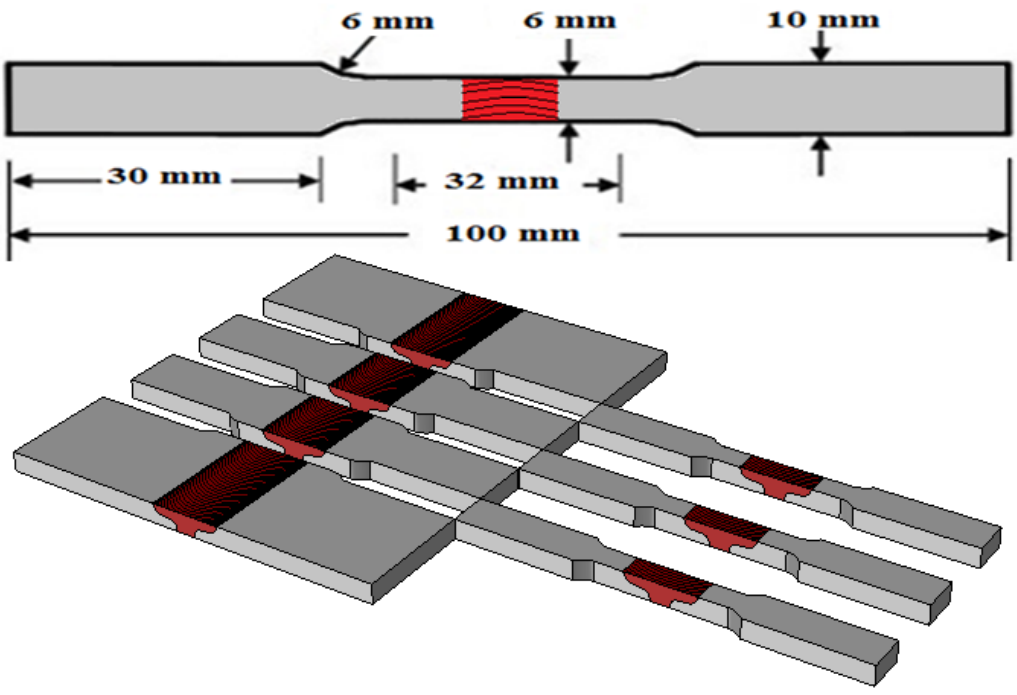

Figure 4. Schematic of tensile test specimens and related cutting position.

To perform the Vickers hardness test, a cross-section for each of the welded specimens was prepared and polished using 220, 320, 500, 800, and 1200 grit sandpapers to test the microhardness. The microhardness test was performed in 30 s under a load of 50 g at room temperature. To record the microhardness distribution for each sample, 16 points were used at a depth of 1.5 mm of the weld section and perpendicular to the weld line with a distance of 1.5 mm. The positions of the points used to measure hardness in the weld have been shown in Figure 5 schematically. Welded samples were subjected to

metallographic tests to investigate microstructural changes. For this purpose, from each of the welded specimens, samples with dimensions of 5 × 5 × 20 mm were cut in the direction perpendicular to the weld line. They were then polished with 400 to 2000 grit sandpaper. For etching, Keller reagent was used with a combination of 1% by volume of hydrofluoric acid, 1.5% by volume of hydrochloric acid, 2.5% by volume of nitric acid, and 95% by volume of distilled water. The samples were etched in the prepared solution for 30 s.

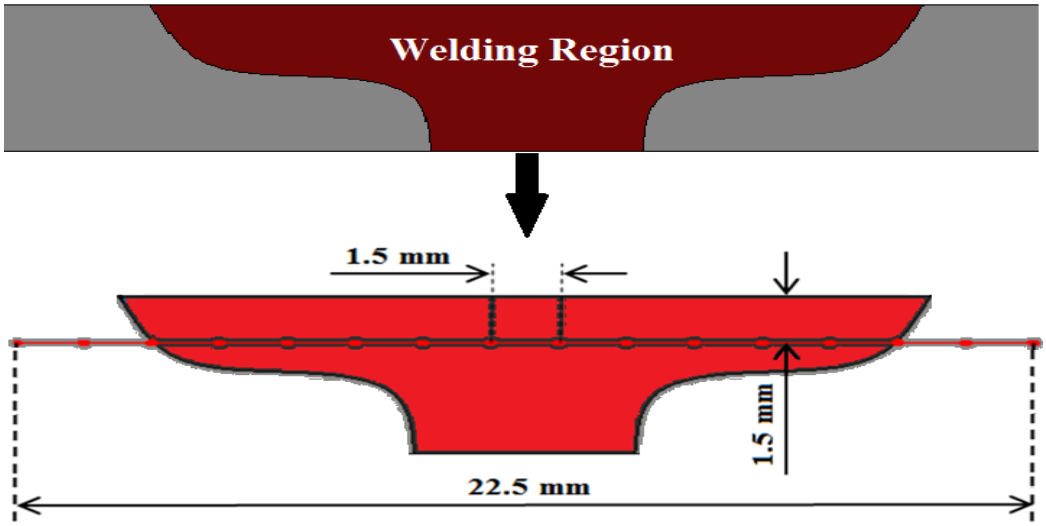

Figure 5. Position of points used for hardness measurement.

3. Results and Discussion

3.1. Surface Morphology and Macrographs of Welding Specimens

Three techniques, FSW, AP-FSW, and RP-FSW, were used to join AA6061-T6 aluminum alloys together. In this section, the surface morphology of welded specimens is first investigated. In Figure 6, the surfaces of welded specimens by three techniques described in different tool offsets have been shown.

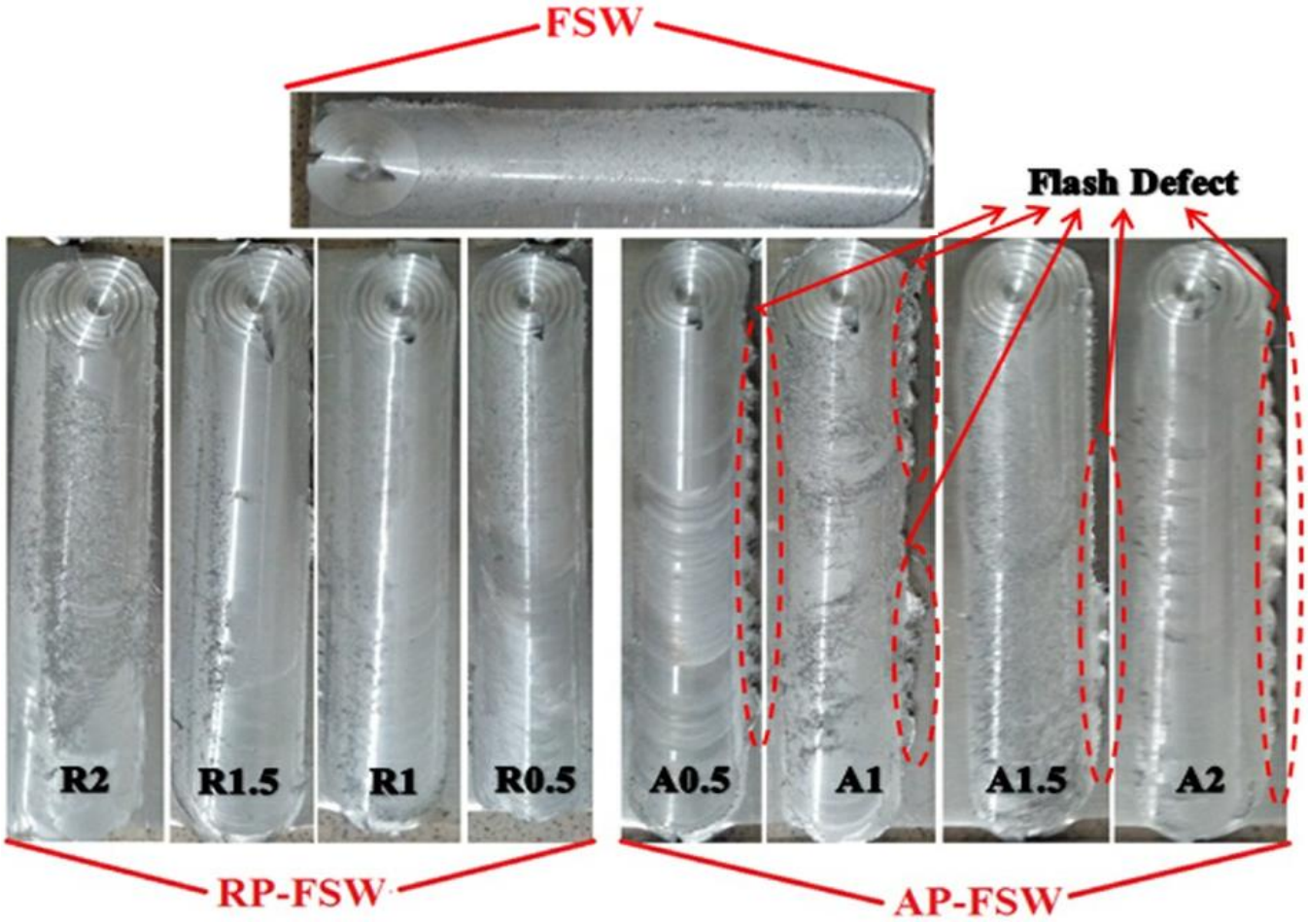

Figure 6. Surfaces of welded specimens by three introduced welding techniques.

As can be seen, the surfaces of all welded specimens with three different techniques are smooth, and there is no defect of lack of fill on the surfaces of the specimens. In FSW and RP-FSW welded specimens, the welded surfaces are smooth and fully integrated, and no visible protrusions or voids were formed in these specimens. However, it can be seen that in all four samples welded by the AP-FSW technique, protrusions and flash have been formed in the marginal area of the welding line. In general, the flash defect is caused by an increase in heat in the area of the welding edges [50–53]. According to the studies conducted in the literature review, the temperature distribution in the AS is larger than the RS, and the maximum process temperature normally occurs in this region [2,54]. Therefore, it was observed that in the samples welded by the AP-FSW technique, due to the accumulation of heat in the nugget zone (AS region) and the increase in heat from the optimal value, flash defects were formed. In RP-FSW welded specimens, the concentration of heat and plastic flow in the central weld zone (RS zone) is more stable, and no significant surface defects were observed in these specimens. In RP-FSW welded specimens, the concentration of heat and plastic flow in the nugget zone (RS zone) is more stable, and no significant surface defects were observed in these specimens. For a more appropriate study, the welding cross-section macrographs of welded specimens by the AP-FSW and RP-FSW methods have been shown in Figure 7.

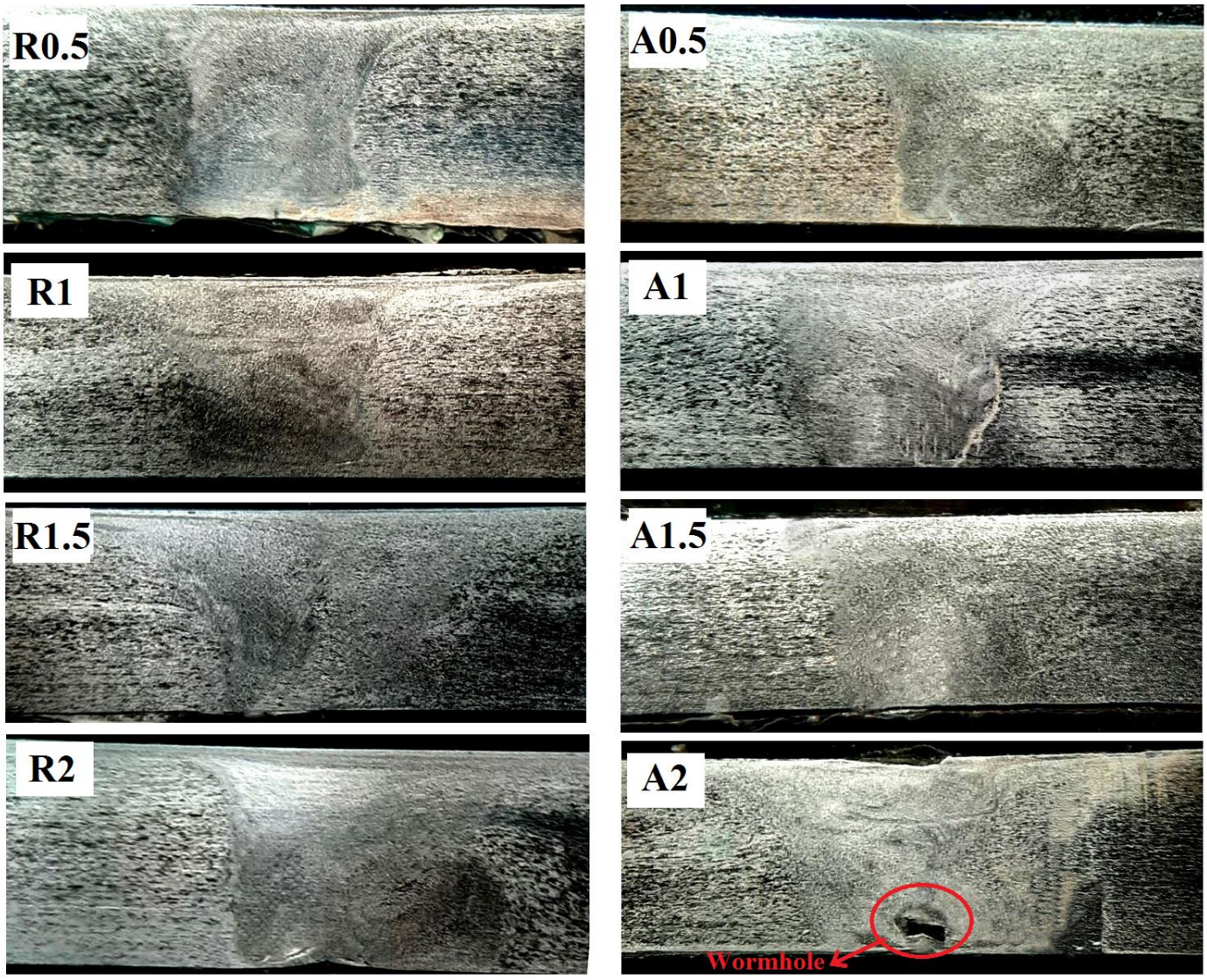

Figure 7. Welded section cross-section macrograph of AP-FSW and RP-FSW samples.

As shown in Figure 7, the cross-section of all welding specimens except the A2 lacks common defects such as voids and wormholes. These two common defects are because of the lack of adequate and improper plastic flow [55–57]. In AP-FSW welded specimens, the direction of material flow is toward the peripheral areas of the welding line, which causes a lack of proper concentration of flow in the central welding area. In sample A2, due to the size of the weld zone caused by the increase in the tool offset and the decrease in the concentration of plastic flow, the bottom surface of the sample has a wormhole defect. In general, the presence of a wormhole defect leads to the formation of macro cracks in this area and greatly reduces the mechanical properties of the welded joint [58–62]. The use of AP-FSW and RP-FSW techniques leads to significant modifications in different welding areas. One of these changes is the increase in the area of the Stir Zone (SZ), which is due to the tool offset at the welding passes. According to Figure 7, in the AP-FSW and RP-FSW processes, the welding area in the welded specimens increased with increasing the tool offset in the first and second passes. In the FSW process, the SZ is generally formed at the tool pin passage locus, and its width is approximately equal to the diameter of the tool pin [8,37,47,63,64]. In P-FSW techniques, in addition to the dimensions of the tool, the width of this area depends on the tool offset in the first and second welding passes. As the tool offset increases, the overlap area of the first and second weld passes decreases and the width of the SZ increases [30,40,65,66]. Changing the direction of flow (advancing

or retreating) and the surface of this region directly leads to changes in the microstructural patterns and mechanical properties of the welding joint.

3.2. Tensile Test Results

According to the explanations provided in Section 2, 27 samples were provided for tensile testing from 9 experimental joints. It should be noted that the average results obtained from three tensile tests were reported as the final results. Four parameters of Yield Stress (YS), Ultimate Tensile Stress (UTS), Elongation Percentage (E%), and failure position of the samples were considered to study. The results obtained from the tensile tests are shown in Table 4.

Table 4. Results of tensile tests.

Process	Sample	YS (MPa)	UTS (MPa)	E%	Fracture Location
	BM	268	311	17	Middle
FSW	Base	132	179	8.3	AS-HAZ
AP-FSW	A0.5	136	185	9.3	SZ
	A1	151	195	9.5	SZ
	A1.5	179	211	10.2	SZ
	A2	125	163	8.4	SZ
RP-FSW	R0.5	150	201	10.8	AS-HAZ
	R1	191	246	11.2	AS-HAZ
	R1.5	205	269	11.9	AS-HAZ
	R2	189	223	11.6	AS-TMAZ

Failure of tensile test specimens may occur mainly in four zones, which are the SZ, Thermo-Mechanically Affected zone (TMAZ), Heat-Affected Zone (HAZ), and the Base Metal (BM), respectively. Depending on the type and connection conditions, the final failure occurs in one of the zones listed in the AS or RS sections. In FSW welded specimens, due to the endurance of large thermal cycles and lack of proper plastic flow in the AS, the final failure generally occurs in this region. Based on the results presented in Table 4, the samples studied in the present study also generally experienced final failure in the AS. Due to the location of the AS in the middle of the welding section of AP-FSW specimens, it can be seen that the specimens welded by this method failed from the central section. In addition, in the samples welded by the RP-FSW method, due to the location of the AS areas at the edge of the workpiece, failure occurred in the edges of the weld line. Based on the results of tensile tests presented in Table 4, in all studied offsets, the UTS, YS, and E% parameters of the joints welded by the RP-FSW technique are larger than the AP-FSW specimens. According to the researches, in general, the mechanical and microstructural properties of the joint in the RS region are more suitable than in the AS region, which is due to the appropriate and significant plastic flow in the RS region compared to the AS [67–69]. Due to the inversion of the flow direction and the direction of tool movement in AS, a relatively fewer material flow is formed in AS than in RS. This leads to a lack of proper microstructure and concentration of defects in this area of the weld, which ultimately reduces the mechanical properties of the final joint. In the RP-FSW process, the central part of the weld line is completely located in the RS region, which increases the mechanical properties of the joint. In Figures 8–10, the diagrams of changes in the YS, UTS, and E% parameters for different specimens have been shown, respectively.

Based on the results presented in Figure 8, it was found that the tool offset in the AP-FSW and RP-FSW processes is the most important factor affecting the mechanical properties of the joint. In both AP-FSW and RP-FSW processes, by increasing the tool offset, the YS parameter experiences a significant increase to an offset of 1.5 mm and then decreases. In the 1.5 mm offset, in the AP-FSW and RP-FSW process, the YS parameter experiences

35.6% and 55.3% growth in comparison with the base specimen (FSW joint), respectively. These significant changes in mechanical properties can be attributed to changes in the heat distribution pattern, material flow pattern, and microstructural changes that occur with changes in the tool offset during the weld zone.

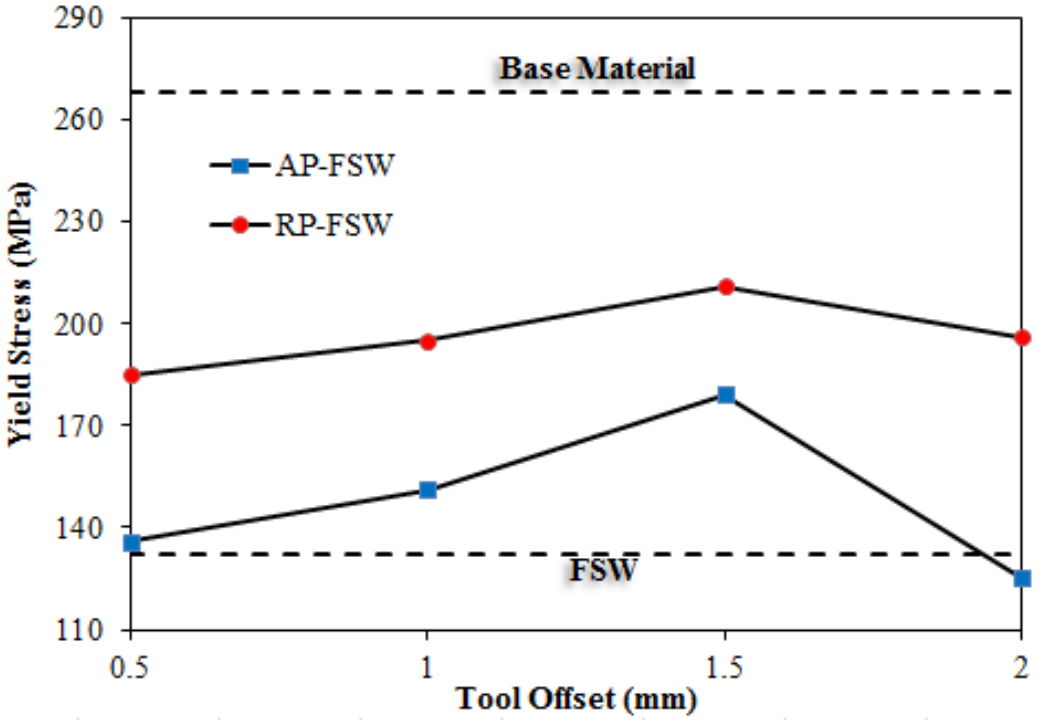

Figure 8. Comparison of YS values of welded specimens with FSW, AP-FSW, and RP-FSW techniques.

According to Figures 9 and 10, a similar pattern is observed in the UTS and E% variables. The final values of these two parameters are also directly dependent on the type of welding process and the tool offset in two welding passes. In samples welded by AP-FSW and RP-FSW methods, the UTS and E% variables were at maximum level at a tool offset of 1.5 mm. In this situation, the UTS and E% parameters for the AP-FSW specimen experienced 17.8% and 50%, respectively, and the RP-FSW specimen experienced 22.8% and 43.3% growth compared to the FSW specimen. In both groups welded by AP-FSW and RP-FSW methods, increasing the tool offset by more than 1.5 mm reduced the joint's mechanical properties.

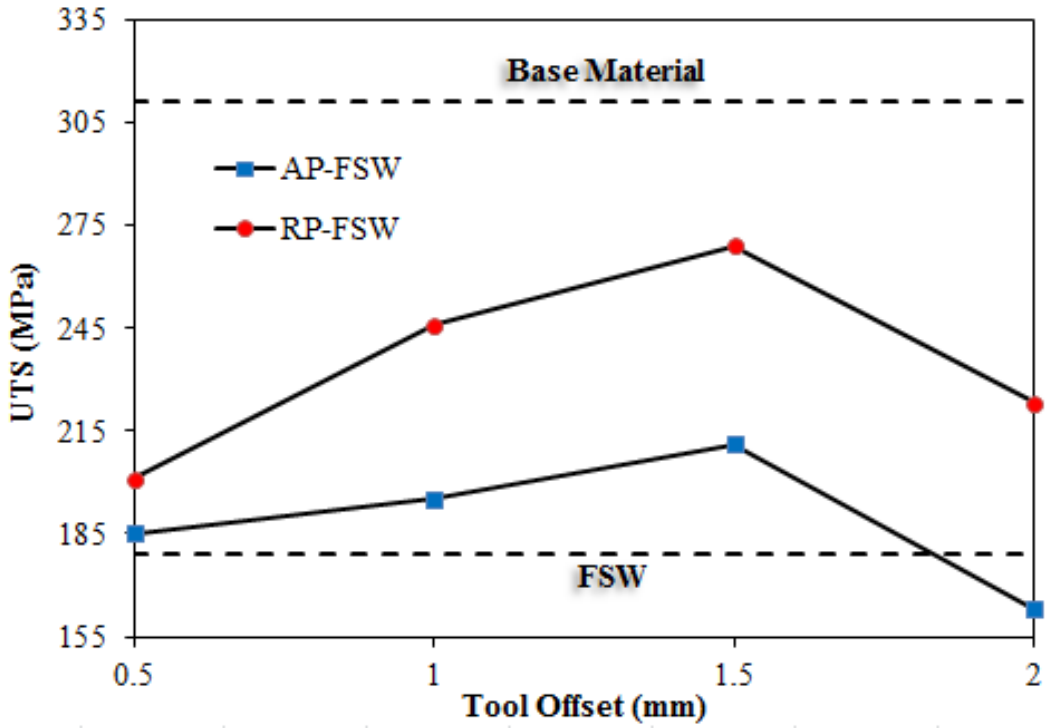

Figure 9. Comparison of UTS values of welded specimens with FSW, AP-FSW, and RP-FSW techniques.

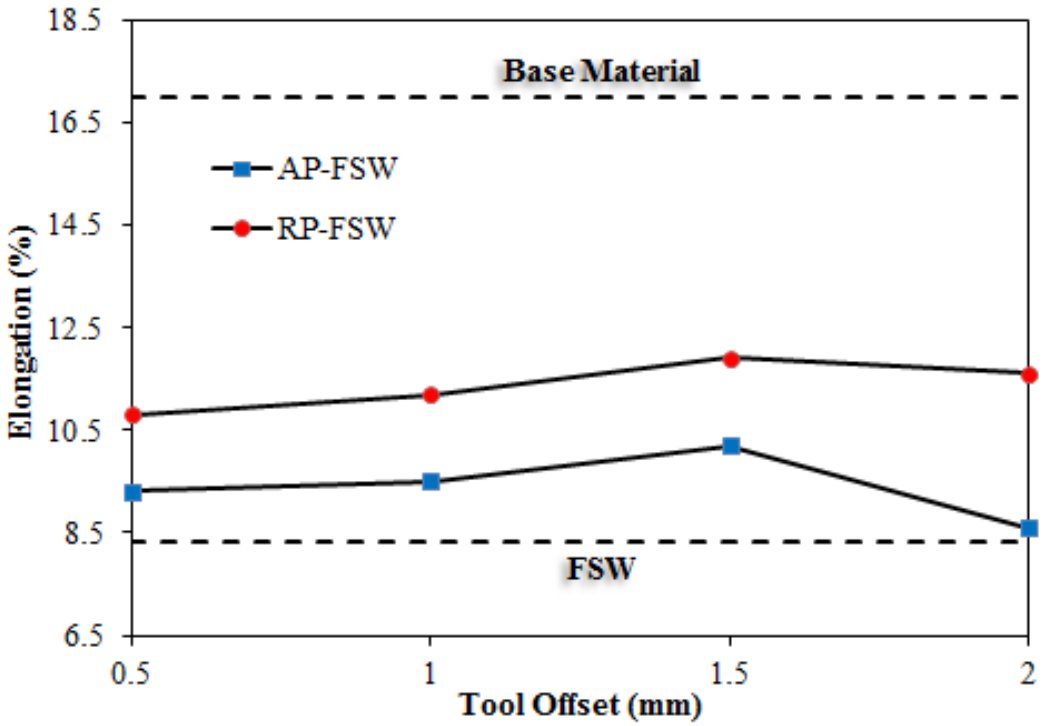

Figure 10. Comparison of E% values of welded specimens with FSW, AP-FSW, and RP-FSW techniques.

This decrease in mechanical properties is due to the reduction in plastic flow concentration in the central area of the weld and the formation of defects in the weld nugget. The lowest tensile mechanical properties among welded specimens using the three methods belong to specimen A2. According to the results, it was found that except for the A2 specimen, the mechanical properties of other joints performed by two processes of AP-FSW

and RP-FSW in all different tool offsets had a significant increase compared to the FSW specimen. According to the presented results, it was found that the use of AP-FSW and RP-FSW methods in comparison with conventional FSW significantly increases the mechanical properties of the joint. The RP-FSW peak model (specimen R1.5) has the closest mechanical properties to the base metal, in which the parameters YS, UTS, and E% are 76.4%, 86.5%, and 70% of the base metal, respectively.

3.3. Microhardness and Microstructure

The microhardness patterns of welded specimens with AP-FSW and RP-FSW techniques with different tool offsets have been shown in Figures 11 and 12, respectively.

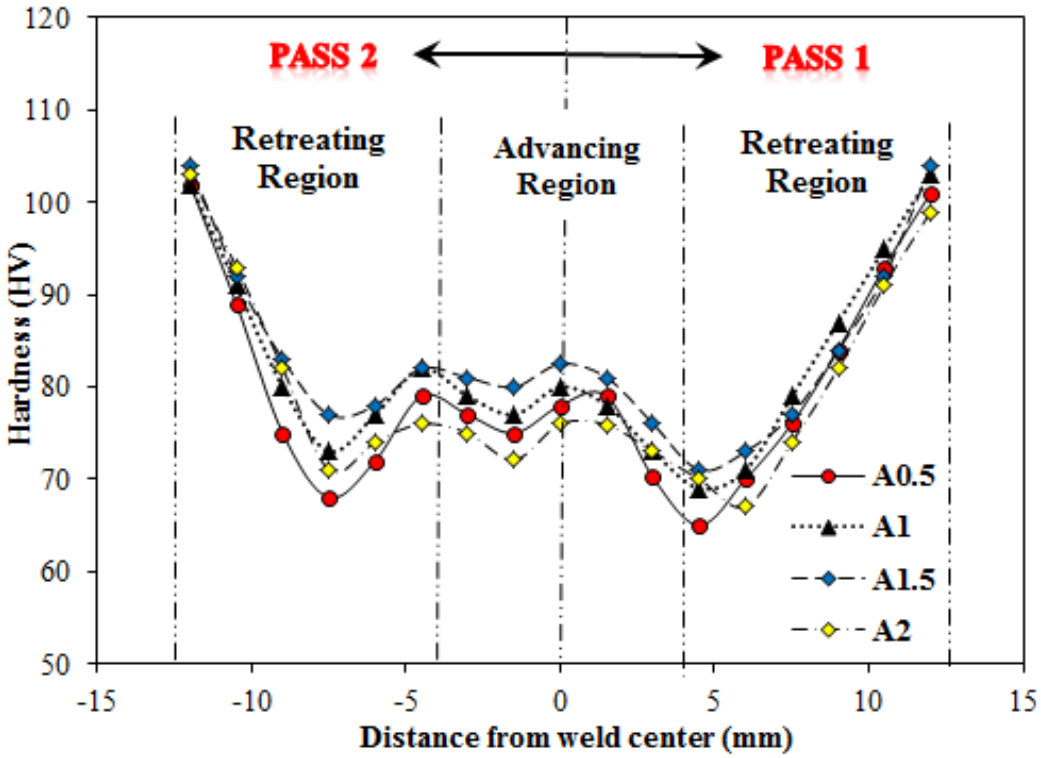

Figure 11. Hardness profiles of AP-FSW specimens with different tool offsets.

According to Figures 12 and 13, regardless of the tool offset, the hardness profiles of the zones located in the first and second passes of specimens welded by AP-FSW and RP-FSW are asymmetric. In both groups of welded specimens, the hardness of the zones covered in the second pass is greater than the zones covered in the first pass. This is due to the intensification of microstructural changes in the zones covered by the second welding pass, which leads to further microstructural corrections and improved hardness of these zones. Hardness changes of welded specimens with two processes of AP-FSW and RP-FSW have a relatively similar pattern. In both groups, the highest hardness belongs to the welded specimens with offsets of 1.5, 1, 0.5, and 2 mm, respectively. The main difference in the stiffness pattern formed in these two processes is related to the weld nugget. The RP-FSW specimens, due to higher material flow concentration and better microstructure modification, had greater hardness in comparison with AP-FSW specimens. According to the diagrams presented in Figures 11 and 12, regardless of the type of welding process, the pattern of microhardness distribution across the weld cross-section of all samples is W-shaped, which is in accordance with the patterns obtained in most FSW studies [65,70,71].

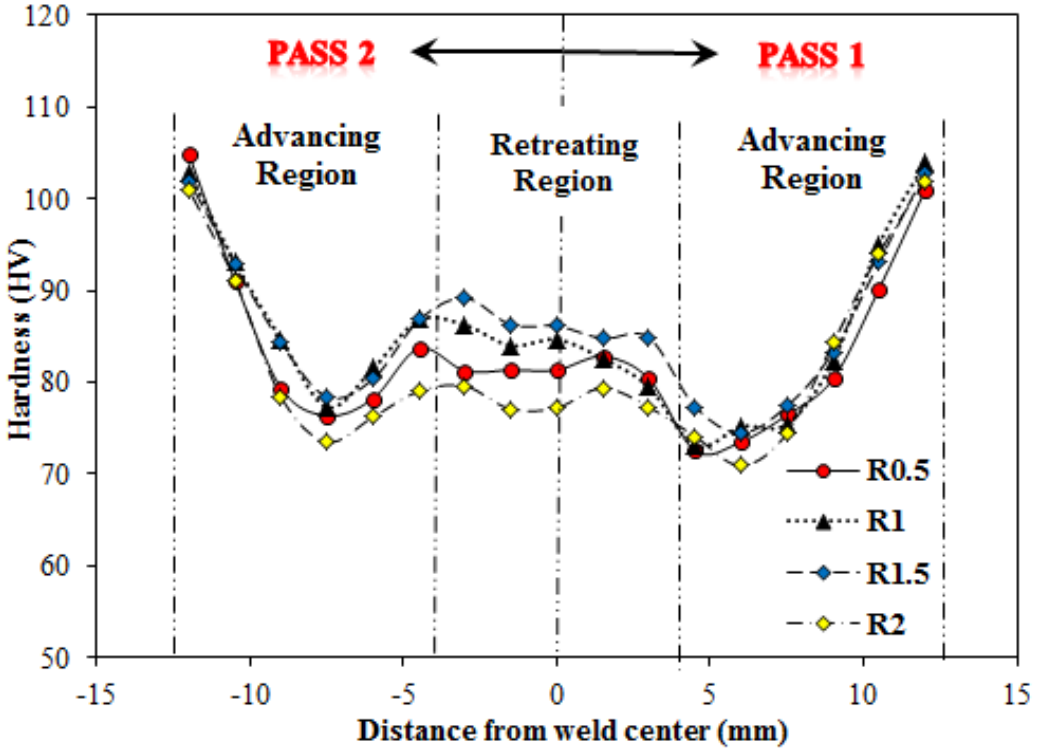

Figure 12. Hardness profiles of RP-FSW specimens with different tool offsets.

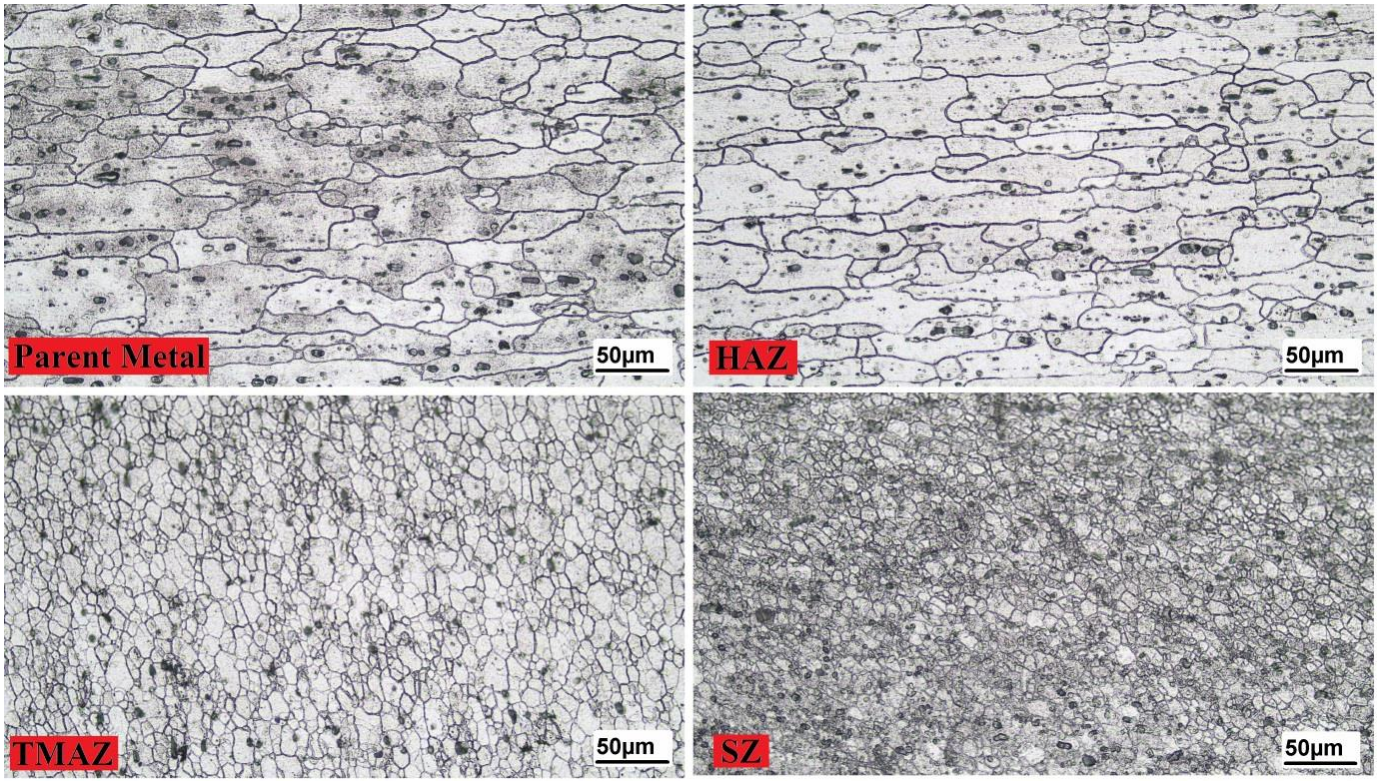

Figure 13. Microstructure of different areas of the sample welded by FSW technique.

In all samples, the lowest hardness values occurred in the HAZ. After the HAZ region, TMAZ and SZ had the least amount of hardness. In the SZ, due to the presence of large plastic flow and heat close to the melting temperature, complete dynamic recrystallization, and more appropriate microstructure modification are formed in this region. Due

to the inverse relationship between hardness and grain size, by reducing the grain size in the SZ, the hardness of this region experiences significant growth compared to other areas of the weld section [2]. The microstructure images of different regions of the FSW welding sample have been shown in Figure 13.

As can be seen, the grain size differentiation in the SZ, TMAZ, and HAZ regions is well marked in the microstructural images. No dynamic recrystallization has taken place in the HAZ, and the grain sizes in this region are almost similar to that of the base metal and are only partially elongated. The TMAZ is formed by high temperature and uniform deformation during the welding process. Deformed and somewhat recrystallized grains can be seen in this zone. Recrystallization is rare in TMAZ due to insufficient temperature and less deformation intensity than in the central region. The SZ has the highest deformation rate among other regions and contains fine and equiaxed grains resulting from complete dynamic recrystallization. This zone experiences the highest temperature and plastic deformation during the process. Severe plastic deformation and high temperature in this area have led to complete recrystallization and severe microstructural changes in this area. As can be seen in Figure 13, in the SZ, relatively microstructural modification and severe being fine-grained have occurred. To compare the difference in grain size in the weld nugget of different samples, the SZ grain size image of welded specimens using the AP-FSW and RP-FSW techniques has been shown in Figure 14. In addition, for the purpose of quantitative comparison, the average grain size diagram of the SZ of welded specimens with three techniques, FSW, AP-FSW, and RP-FSW, has been shown in Figure 15.

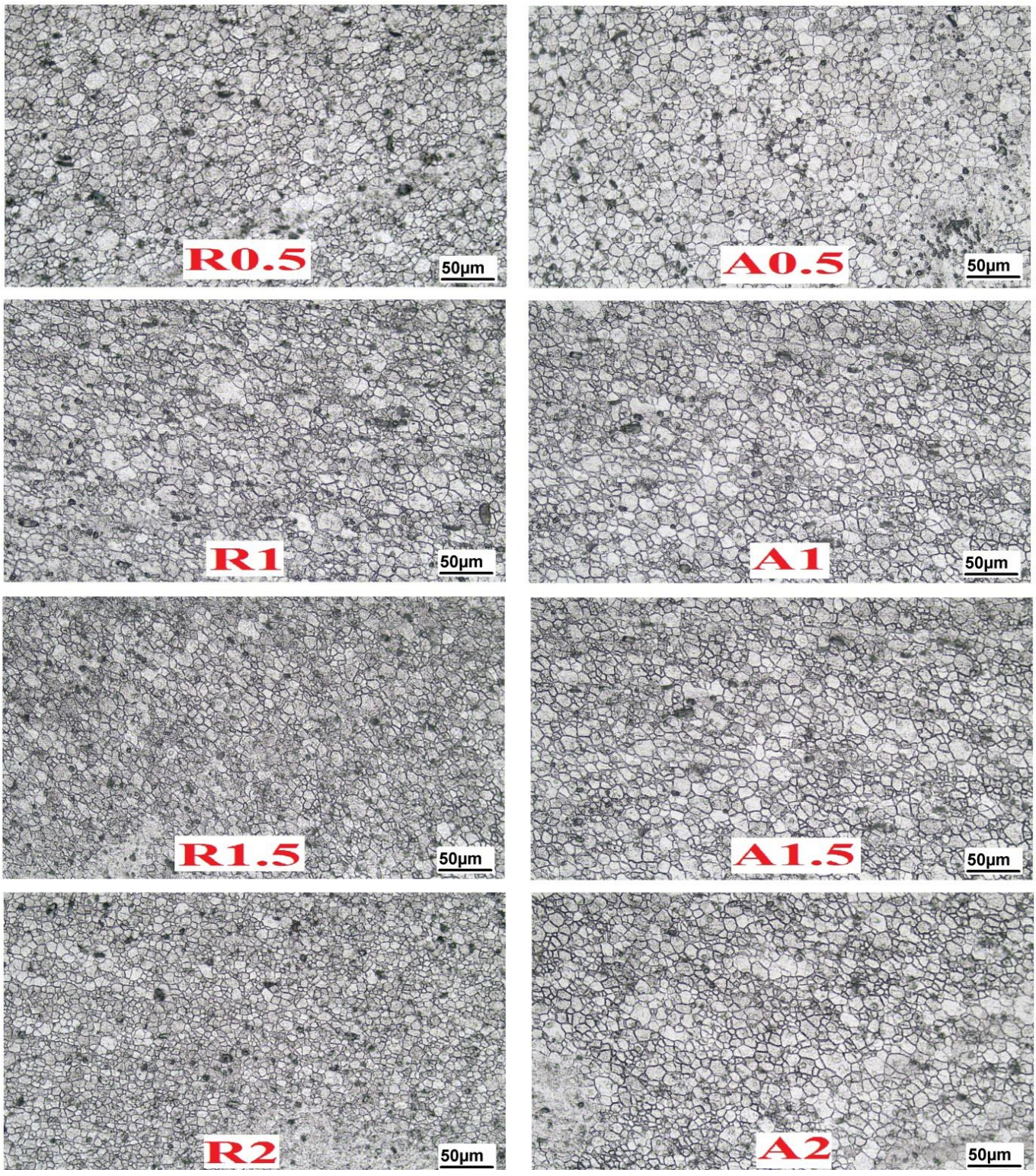

Figure 14. Distribution of SZ microstructure for welded specimens using AP-FSW and RP-FSW techniques.

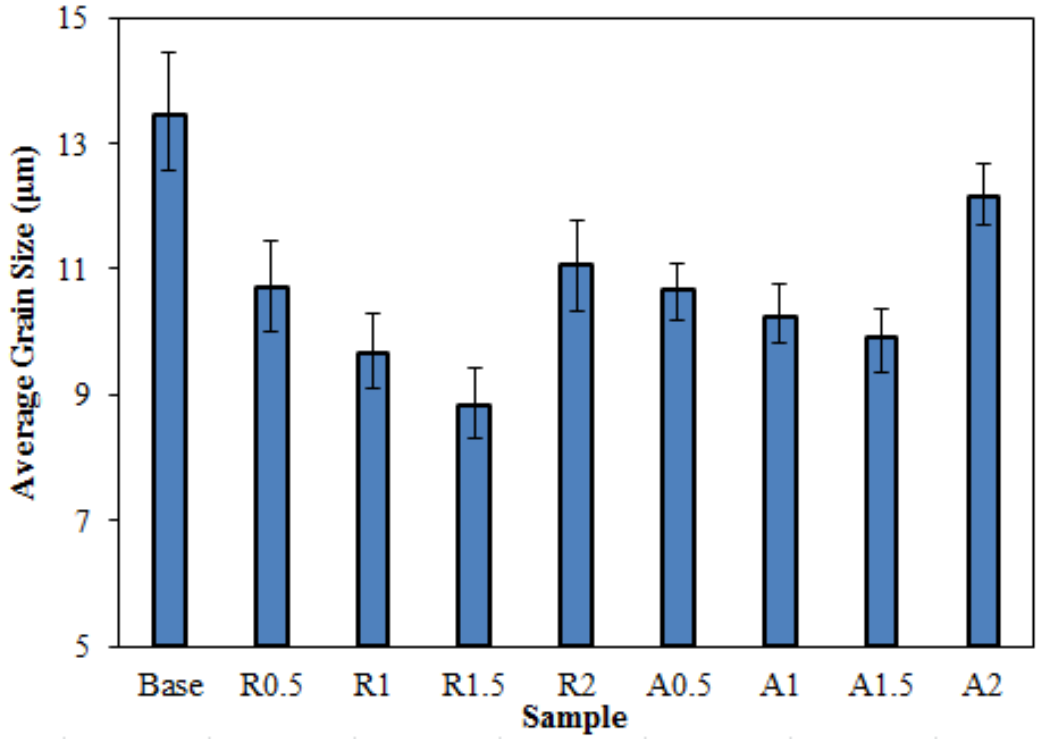

Figure 15. Comparison of average SZ grain size of welded specimens.

As shown in Figures 14 and 15, the lowest grain size in the SZ region belongs to the samples welded by RP-FSW, AP-FSW, and FSW methods, respectively. It can be seen that the trend in the average grain size in the three welding methods is in accordance with the results obtained from tensile and microhardness tests. In the samples welded by AP-FSW and RP-FSW methods, due to the overlap formed in the first and second passes, the microstructural modification increased, which resulted in increasing the being fine-grained in the SZ. As can be seen, up to 1.5 mm tool offset, the mean grain size in the SZ is inversely proportional to the tool offset value in the first and second passes. As the tool offset increases, due to the reduction in the area of the overlap region in the first and second passes and the reduction in severe plastic deformation and heat in this region, the phenomenon of crystallized grain growth decreases, and finally, this process leads to a decrease in average grain size. The lowest average grain size belongs to the sample R1.5. The average grain size in this sample has decreased by 34.4% compared to the FSW sample. The reason for the differences in mechanical properties and microstructure of specimens welded with introduced three methods used is the different nature of these methods. In the conventional FSW method, due to the non-uniformity of the translational and rotational speeds directions of the tool on both sides of the welding line, the material flow and temperature distribution have an asymmetric trend in the process. This asymmetry in the process leads to the formation of fundamental differences in the RS and AS. Using AP-FSW and RP-FSW techniques, the temperature, and material flow distribution patterns change from an asymmetric condition to a relatively symmetrical one, and the regions formed in the welding section have similar and balanced conditions on both sides of the weld line.

4. Conclusions

The present study investigated the effect of two parameters of process type and tool offset value on tensile, microhardness, and microstructure properties of AA6061-T6 aluminum alloy joints. Three methods were used: FSW, AP-FSW, and RP-FSW. The following results were obtained:

1. In both AP-FSW and RP-FSW processes, the mechanical properties of the joint in most of the tool offset values significantly increased compared to the FSW process, which indicates the superiority of the joint in P-FSW processes over conventional FSW.
2. In all tool offset values, the mechanical properties and efficiencies of the joints formed by the RP-FSW technique were greater than those of the AP-FSW specimens.
3. In both AP-FSW and RP-FSW processes, the UTS, YS, and E% of welded specimens increased by increasing the tool offset up to 1.5 mm. The best mechanical properties for both AP-FSW and RP-FSW processes were formed at the tool offset of 1.5 mm.
4. At the tool offset of 1.5 mm, in the AP-FSW and RP-FSW processes, the YS parameter grew 35.6% and 55.3% relative to the base sample (FSW joint), and the UTS parameter relative to the base sample (FSW joint) experienced 17.8% and 50.2% increase, respectively.
5. The peak sample of the RP-FSW process (1.5 mm of tool offset) had the closest mechanical properties to the base metal. In this sample, the parameters YS, UTS, and E% are 76.4%, 86.5%, and 70% of the base metal values, respectively.
6. The failure position of the welding specimens in the tensile test was significantly dependent on the type of welding process. In all welded specimens using FSW, RP-FSW, and AP-FSW techniques, specimen failure occurred in the AS.
7. Regardless of the type of welding process, the lowest hardness values occurred in the HAZ in all specimens. After HAZ, TMAZ and SZ had the lowest hardness compared to the hardness of the base material.
8. RP-FSW welded specimens had more suitable microstructure modification, finer grain size, and higher hardness values compared to AP-FSW specimens.

Author Contributions: Conceptualization, A.G., M.M.Y., J.T., H.K., A.D., S.M. and H.A.D.; methodology, A.G., M.M.Y., H.K., A.D., and S.M.; software, A.G., M.M.Y., J.T., J.W.G.G., and H.K.; validation, A.G., M.M.Y., H.K., A.D., J.W.G.G., and S.M.; formal analysis, A.G., M.M.Y., J.T., H.K., A.D., S.M., and H.A.D.; investigation, A.G., M.M.Y., H.K., A.D., and S.M.; writing—original draft preparation, A.G., M.M.Y., J.T., H.K., A.D., S.M., and H.A.D.; writing—review and editing, A.G., M.M.Y., J.T., H.K., A.D., S.M., J.W.G.G., and H.A.D.; visualization, A.G., M.M.Y., J.T., H.K., A.D., S.M., and H.A.D.; supervision, A.G.; project administration, A.G. All authors have read and agreed to the published version of the manuscript.

Funding: This research received no external funding.

Institutional Review Board Statement: Not applicable.

Informed Consent Statement: Not applicable.

Data Availability Statement: Data sharing is not applicable to this article.

Conflicts of Interest: The authors declare no conflict of interest.

References

1. Derazkola, H.A.; Khodabakhshi, F.; Gerlich, A. Friction-forging tubular additive manufacturing (FFTAM): A new route of solid-state layer-upon-layer metal deposition. *J. Mater. Res. Technol.* **2020**, *9*, 15273–15285, doi:10.1016/j.jmrt.2020.10.105.
2. Derazkola, H.A.; Simchi, A. A new procedure for the fabrication of dissimilar joints through injection of colloidal nanoparticles during friction stir processing: Proof concept for AA6062/PMMA joints. *J. Manuf. Process.* **2020**, *49*, 335–343, doi:10.1016/j.jmapro.2019.12.008.
3. Derazkola, H.A.; Simchi, A. Processing and characterizations of polycarbonate/alumina nanocomposites by additive powder fed friction stir processing. *Thin-Walled Struct.* **2020**, *157*, 107086, doi:10.1016/j.tws.2020.107086.
4. Derazkola, H.A.; Khodabakhshi, F. Development of fed friction-stir (FFS) process for dissimilar nanocomposite welding between AA2024 aluminum alloy and polycarbonate (PC). *J. Manuf. Process.* **2020**, *54*, 262–273, doi:10.1016/j.jmapro.2020.03.020.
5. Babu, S.D.D.; Sevvel, P.; Kumar, R.S.; Vijayan, V.; Subramani, J. Development of Thermo Mechanical Model for Prediction of Temperature Diffusion in Different FSW Tool Pin Geometries During Joining of AZ80A Mg Alloys. *J. Inorg. Organomet. Polym. Mater.* **2021**, *31*, 1–17, doi:10.1007/s10904-021-01931-4.
6. Babu, S.D.D.; Sevvel, P.; Kumar, R.S. Simulation of heat transfer and analysis of impact of tool pin geometry and tool speed during friction stir welding of AZ80A Mg alloy plates. *J. Mech. Sci. Technol.* **2020**, *34*, 4239–4250, doi:10.1007/s12206-020-0916-7.

7. Sevvel, P.; Babu, S.D.; Kumar, R.S. Peak Temperature Correlation and Temperature Distribution during Joining of AZ80A Mg Alloy by FSW – A Numerical and Experimental Investigation. *Stroj. Vestn. J. Mech. Eng.* **2020**, *66*, 395–407, doi:10.5545/sv-jme.2020.6566.
8. Satheesh, C.; Sevvel, P.; Senthil Kumar, R. Experimental Identification of Optimized Process Parameters for FSW of AZ91C Mg Alloy Using Quadratic Regression Models. *Stroj. Vestn. J. Mech. Eng.* **2020**, *66*, 736–751, doi:10.5545/sv-jme.2020.6929.
9. Ghiasvand, A.; Kazemi, M.; Jalilian, M.M.; Rashid, H.A. Effects of tool offset, pin offset, and alloys position on maximum temperature in dissimilar FSW of AA6061 and AA5086. *Int. J. Mech. Mater. Eng.* **2020**, *15*, 1–14, doi:10.1186/s40712-020-00118-y.
10. Akbari, M.; Aliha, M.; Keshavarz, S.; Bonyadi, A. Effect of tool parameters on mechanical properties, temperature, and force generation during FSW. *Proc. Inst. Mech. Eng. Part L: J. Mater. Des. Appl.* **2019**, *233*, 1033–1043, doi:10.1177/1464420716681591.
11. Paidar, M.; Mehrez, S.; Babaei, B.; Memon, S.; Ojo, O.; Lankarani, H. Dissimilar welding of AA5083 to AZ31 Mg alloys using modified friction stir clinching brazing. *Mater. Lett.* **2021**, *301*, 129764, doi:10.1016/j.matlet.2021.129764.
12. Mehta, K.P.; Patel, R.; Vyas, H.; Memon, S.; Vilaça, P. Repairing of exit-hole in dissimilar Al-Mg friction stir welding: Process and microstructural pattern. *Manuf. Lett.* **2020**, *23*, 67–70, https://doi.org/10.1016/j.mfglet.2020.01.002.
13. Paidar, M.; Memon, S.; Samusenkov, V.O.; Babaei, B.; Ojo, O.O. Friction spot extrusion welding-brazing of copper to aluminum alloy. *Mater. Lett.* **2021**, *285*, 129160, https://doi.org/10.1016/j.matlet.2020.129160.
14. Memon, S.; Paidar, M.; Mehta, K.P.; Babaei, B.; Lankarani, H.M. Friction Spot Extrusion Welding on Dissimilar Materials AA2024-T3 to AA5754-O: Effect of Shoulder Plunge Depth. *J. Mater. Eng. Perform.* **2021**, *30*, 334–345, 10.1007/s11665-020-05387-4.
15. Memon, S.; Paidar, M.; Mehrez, S.; Cooke, K.; Ojo, O.O.; Lankarani, H.M. Effects of materials positioning and tool rotational speed on metallurgical and mechanical properties of dissimilar modified friction stir clinching of AA5754-O and AA2024-T3 sheets. *Results Phys.* **2021**, *22*, 103962, https://doi.org/10.1016/j.rinp.2021.103962.
16. Memon, S.; Fydrych, D.; Fernandez, A.C.; Derazkola, H.A.; Derazkola, H.A. Effects of FSW Tool Plunge Depth on Properties of an Al-Mg-Si Alloy T-Joint: Thermomechanical Modeling and Experimental Evaluation. *Materials* **2021**, *14*, 4754.
17. Memon, S.; Tomków, J.; Derazkola, H.A. Thermo-Mechanical Simulation of Underwater Friction Stir Welding of Low Carbon Steel. *Materials.* **2021**, *14*, 4953.
18. Memon, S.; Murillo-Marrodán, A.; Lankarani, H.M.; Aghajani Derazkola, H. Analysis of Friction Stir Welding Tool Offset on the Bonding and Properties of Al–Mg–Si Alloy T-Joints. *Materials.* **2021**, *14*, 3604.
19. Dialami, N.; Cervera, M.; Chiumenti, M. Effect of the Tool Tilt Angle on the Heat Generation and the Material Flow in Friction Stir Welding. *Metals.* **2019**, *9*, 28.
20. Derazkola, H.A.; Simchi, A. An investigation on the dissimilar friction stir welding of T-joints between AA5754 aluminum alloy and poly(methyl methacrylate). *Thin-Walled Struct.* **2019**, *135*, 376–384, https://doi.org/10.1016/j.tws.2018.11.027.
21. Zhao, Z.; Liang, H.; Zhao, Y.; Yan, K. Effect of Exchanging Advancing and Retreating Side Materials on Mechanical Properties and Electrochemical Corrosion Resistance of Dissimilar 6013-T4 and 7003 Aluminum Alloys FSW Joints. *J. Mater. Eng. Perform.* **2018**, *27*, 1777–1783, https://doi.org/10.1007/s11665-018-3253-6.
22. Aghajani Derazkola, H.; Garcia, E.; Elyasi, M. Underwater friction stir welding of PC: Experimental study and thermo-mechanical modelling. *J. Manuf. Process.* **2021**, *65*, 161–173, https://doi.org/10.1016/j.jmapro.2021.03.034.
23. Derazkola, H.A.; Elyasi, M. The influence of process parameters in friction stir welding of Al-Mg alloy and polycarbonate. *J. Manuf. Process.* **2018**, *35*, 88–98, https://doi.org/10.1016/j.jmapro.2018.07.021.
24. Guerra, M.; Schmidt, C.; McClure, J.C.; Murr, L.E.; Nunes, A.C. Flow patterns during friction stir welding. *Mater. Charact.* **2002**, *49*, 95–101, https://doi.org/10.1016/S1044-5803(02)00362-5.
25. Elyasi, M.; Derazkola, H.A.; Hosseinzadeh, M. Investigations of tool tilt angle on properties friction stir welding of A441 AISI to AA1100 aluminium. *Proceed. Inst. Mech. Part B.* **2016**, *320*, 1234–1241, https://doi.org/ 10.1177/0954405416645986.
26. Derazkola, H.A.; Eyvazian, A.; Simchi, A. Modeling and experimental validation of material flow during FSW of polycarbonate. *Mater. Today Commun.* **2020**, *22*, https://doi.org/10.1016/j.mtcomm.2019.100796.
27. Alebizadehsardari, P.; Musharavati, F.; Khan, F.; Sebaey, T.A.; Eyvaziana, A.; Derazkola, H.A. Underwater friction stir welding of Al-Mg alloy: Thermo-mechanical modeling and validation. *J. Mater. Today. Commun.* **2021**, *26*, 101965, https://doi.org/10.1016/j.mtcomm.2020.101965.
28. Aghajani Derazkola, H.; Simchi, A. Effects of alumina nanoparticles on the microstructure, strength and wear resistance of poly(methyl methacrylate)-based nanocomposites prepared by friction stir processing. *J. Mech. Behav. Biomed. Mater.* **2018**, *79*, https://doi.org/10.1016/j.jmbbm.2018.01.007.
29. Xu, X.; Zhang, C.; Derazkola, H.A.; Demiral, M.; Zain, A.M.; Khan, A. UFSW tool pin profile effects on properties of aluminium-steel joint. *Vacuum* **2021**, *192*, 110460, https://doi.org/10.1016/j.vacuum.2021.110460.
30. Sharma, A.; Morisada, Y.; Fujii, H. Influence of aluminium-rich intermetallics on microstructure evolution and mechanical properties of friction stir alloyed AlFe alloy system. *J. Manuf. Process.* **2021**, *68*, 668–682, https://doi.org/10.1016/j.jmapro.2021.05.073.
31. Wang, Q.; Zhao, Z.; Zhao, Y.; Yan, K.; Zhang, H. The adjustment strategy of welding parameters for spray formed 7055 aluminum alloy underwater friction stir welding joint. *Mater. Des.* **2015**, *88*, 1366–1376, https://doi.org/10.1016/j.matdes.2015.09.038.
32. Li, J.Q.; Liu, H.J. Characteristics of the reverse dual-rotation friction stir welding conducted on 2219-T6 aluminum alloy. *Mater. Des.* **2013**, *45*, 148–154, https://doi.org/10.1016/j.matdes.2012.08.068.

33. Li, J.Q.; Liu, H.J. Effects of the Reversely Rotating Assisted Shoulder on Microstructures During the Reverse Dual-rotation Friction Stir Welding. *J. Mater. Sci. Technol.* **2015**, *31*, 375–383, https://doi.org/10.1016/j.jmst.2014.07.020.
34. Wang, J.; Cheng, Y.; Li, B.; Chen, C. Effects of Multi-Pass Friction Stir Processing on Microstructures and Mechanical Properties of the 1060Al/Q235 Composite Plate. *Metals.* **2020**, *10*, 298.
35. Ghangas, G.; Singhal, S. Investigations of Multi-pass Friction Stir Welding for Al-Zn-Mg Alloy. *Mater. Today Proc.* **2018**, *5*, 17107–17113, https://doi.org/10.1016/j.matpr.2018.04.118.
36. Brown, R.; Tang, W.; Reynolds, A.P. Multi-pass friction stir welding in alloy 7050-T7451: Effects on weld response variables and on weld properties. *Mater. Sci. Eng. A* **2009**, *513–514*, 115–121, https://doi.org/10.1016/j.msea.2009.01.041.
37. Su, H.; Wu, C. Numerical Simulation for the Optimization of Polygonal Pin Profiles in Friction Stir Welding of Aluminum. *Acta Metall. Sin. English Lett.* **2021**, https://doi.org/10.1007/s40195-021-01198-1.
38. Shi, L.; Wu, C.S.; Liu, H.J. The effect of the welding parameters and tool size on the thermal process and tool torque in reverse dual-rotation friction stir welding. *Int. J. Mach. Tools Manuf.* **2015**, *91*, 1–11, https://doi.org/10.1016/j.ijmachtools.2015.01.004.
39. Liu, H.; Zhang, H. Repair welding process of friction stir welding groove defect. *Trans. Nonferrous Met. Soc. China* **2009**, *19*, 563–567, https://doi.org/10.1016/S1003-6326(08)60313-1.
40. Kumari, K.; Pal, S.K.; Singh, S.B. Friction stir welding by using counter-rotating twin tool. *J. Mater. Process. Technol.* **2015**, *215*, 132–141, https://doi.org/10.1016/j.jmatprotec.2014.07.031.
41. Jain, R.; Kumari, K.; Pal, S.K.; Singh, S.B. Counter rotating twin-tool system in friction stir welding process: A simulation study. *J. Mater. Process. Technol.* **2018**, *255*, 121–128, https://doi.org/10.1016/j.jmatprotec.2017.11.043.
42. Ghiasvand, A.; Hassanifard, S.; Jalilian, M.M.; Kheradmandan, H. Investigation of tool offset on mechanical properties of dissimilar AA6061-T6 and AA7075-T6 joint in parallel FSW process. *Weld. World* **2021**, *65*, 441–450, https://doi.org/10.1007/s40194-020-01037-4.
43. Jesus, J.S.; Costa, J.M.; Loureiro, A.; Ferreira, J.M. Assessment of friction stir welding aluminium T-joints. *J. Mater. Process. Technol.* **2018**, *255*, 387–399, https://doi.org/10.1016/j.jmatprotec.2017.12.036.
44. Tiwari, A.; Pankaj, P.; Suman, S.; Biswas, P. CFD Modelling of Temperature Distribution and Material Flow Investigation During FSW of DH36 Shipbuilding Grade Steel. *Trans. Indian Inst. Met.* **2020**, *73*, 2291–2307, https://doi.org/10.1007/s12666-020-02030-7.
45. Kesharwani, R.; Imam, M.; Sarkar, C. Clarification on the choice of sheet positioning in friction stir welding of dissimilar materials. *Manuf. Lett.* **2020**, *24*, 100–104, https://doi.org/10.1016/j.mfglet.2020.04.008.
46. Zhang, Y.N.; Cao, X.; Larose, S.; Wanjara, P. Review of tools for friction stir welding and processing. *Can. Metall. Q.* **2012**, *51*, 250–261, https://doi.org/10.1179/1879139512Y.0000000015.
47. Gadakh, V.S.; Kumar, A. Friction stir welding window for AA6061-T6 aluminium alloy. *Proc. Inst. Mech. Eng. Part B J. Eng. Manuf.* **2013**, *228*, 1172–1181, https://doi.org/10.1177/0954405413510289.
48. Aghajani Derazkola, H.; Kordani, N.; Aghajani Derazkola, H. Effects of friction stir welding tool tilt angle on properties of Al-Mg-Si alloy T-joint. *CIRP J. Manuf. Sci. Technol.* **2021**, *33*, 264–276, https://doi.org/10.1016/j.cirpj.2021.03.015.
49. Aghajani Derazkola, H.; Simchi, A. Experimental and thermomechanical analysis of friction stir welding of poly(methyl methacrylate) sheets. *Sci. Technol. Weld. Join.* **2017**, https://doi.org/10.1080/13621718.2017.1364896.
50. Ajri, A.; Shin, Y.C. Investigation on the Effects of Process Parameters on Defect Formation in Friction Stir Welded Samples Via Predictive Numerical Modeling and Experiments. *J. Manuf. Sci. Eng.* **2017**, *139*, https://doi.org/10.1115/1.4037240.
51. Ranjan, R.; Khan, A.R.; Parikh, C.; Jain, R.; Mahto, R.P.; Pal, S.; Pal, S.K.; Chakravarty, D. Classification and identification of surface defects in friction stir welding: An image processing approach. *J. Manuf. Process.* **2016**, *22*, 237–253, https://doi.org/10.1016/j.jmapro.2016.03.009.
52. Tamadon, A.; Pons, D.J.; Clucas, D. Flow-Based Anatomy of Bobbin Friction-Stirred Weld; AA6082-T6 Aluminium Plate and Analogue Plasticine Model. *Appl. Mech.* **2020**, *1*, 3–19.
53. Tamadon, A.; Pons, D.J.; Clucas, D. AFM Characterization of Stir-Induced Micro-Flow Features within the AA6082-T6 BFSW Welds. *Technol.* **2019**, *7*, 80.
54. Aghajani Derazkola, H.; Simchi, A.; Lambiase, F. Friction stir welding of polycarbonate lap joints: Relationship between processing parameters and mechanical properties. *Polym. Test.* **2019**, *79*, 105999, https://doi.org/10.1016/j.polymertesting.2019.105999.
55. Mirzaei, M.; Asadi, P.; Fazli, A. Effect of Tool Pin Profile on Material Flow in Double Shoulder Friction Stir Welding of AZ91 Magnesium Alloy. *Int. J. Mech. Sci.* **2020**, *183*, 105775, https://doi.org/10.1016/j.ijmecsci.2020.105775.
56. Meng, X.; Huang, Y.; Cao, J.; Shen, J.; dos Santos, J.F. Recent progress on control strategies for inherent issues in friction stir welding. *Prog. Mater. Sci.* **2021**, *115*, 100706, https://doi.org/10.1016/j.pmatsci.2020.100706.
57. Guan, M.; Wang, Y.; Huang, Y.; Liu, X.; Meng, X.; Xie, Y.; Li, J. Non-weld-thinning friction stir welding. *Mater. Lett.* **2019**, *255*, 126506, https://doi.org/10.1016/j.matlet.2019.126506.
58. Rajendran, C.; Srinivasan, K.; Balasubramanian, V.; Balaji, H.; Selvaraj, P. Effect of tool tilt angle on strength and microstructural characteristics of friction stir welded lap joints of AA2014-T6 aluminum alloy. *Trans. Nonferrous Met. Soc. China* **2019**, *29*, 1824–1835, https://doi.org/10.1016/S1003-6326(19)65090-9.
59. Wang, Z.; Wang, X.; Zhu, Z. Characterization of high-temperature deformation behavior and processing map of TB17 titanium alloy. *J. Alloys Compd.* **2017**, *692*, 149–154, https://doi.org/10.1016/j.jallcom.2016.09.012.

60. Vigneshkumar, M.; Padmanaban, G.; Balasubramanian, V. Influence of Tool Tilt Angle on the Formation of Friction Stir Processing Zone in Cast Magnesium Alloy ZK60/SiCp Surface Composites. *Metallogr. Microstruct. Anal.* **2019**, *8*, 58–66, https://doi.org/10.1007/s13632-018-0507-5.
61. Long, L.; Chen, G.; Zhang, S.; Liu, T.; Shi, Q. Finite-element analysis of the tool tilt angle effect on the formation of friction stir welds. *J. Manuf. Process.* **2017**, *30*, 562–569, https://doi.org/10.1016/j.jmapro.2017.10.023.
62. Donati, L.; Tomesani, L.; Morri, A. Structural T-joint produced by means of friction stir welding (FSW) with filling material. *Int. J. Mater. Form.* **2009**, *2*, 295, https://doi.org/10.1007/s12289-009-0439-3.
63. Amini, S.; Amiri, M.R.; Barani, A. Investigation of the effect of tool geometry on friction stir welding of 5083-O aluminum alloy. *Int. J. Adv. Manuf. Technol.* **2015**, *76*, 255–261, https://doi.org/10.1007/s00170-014-6277-6.
64. Sabari, S.S.; Malarvizhi, S.; Balasubramanian, V. The effect of pin profiles on the microstructure and mechanical properties of underwater friction stir welded AA2519-T87 aluminium alloy. *Int. J. Mech. Mater. Eng.* **2016**, *11*, 5, https://doi.org/10.1186/s40712-016-0058-y.
65. Sun, T.; Roy, M.J.; Strong, D.; Simpson, C.; Withers, P.J.; Prangnell, P.B. Weld zone and residual stress development in AA7050 stationary shoulder friction stir T-joint weld. *J. Mater. Process. Technol.* **2019**, *263*, 256–265, https://doi.org/10.1016/j.jmatprotec.2018.08.022.
66. Zeng, S.; Chen, G.; Dinaharan, I.; Liu, Q.; Zhang, S.; Sahu, P.K.; Wu, J.; Zhang, G.; Shi, Q. Microstructure and Tensile Strength of AA6082 T-joints by Corner Stationary Shoulder Friction Stir Welding: Effect of Tool Rotation Speed. *J. Mater. Eng. Perform.* **2020**, *29*, 7094–7103, https://doi.org/10.1007/s11665-020-05179-w.
67. Derazkola, H.A.; Aval, H.J.; Elyasi, M. Analysis of process parameters effects on dissimilar friction stir welding of AA1100 and A441 AISI steel. *Sci. Technol. Weld. Join.* **2015**, *20*, https://doi.org/10.1179/1362171815Y.0000000038.
68. Khodabakhshi, F.; Derazkola, H.A.; Gerlich, A.P. Monte Carlo simulation of grain refinement during friction stir processing. *J. Mater. Sci.* **2020**, *55*, 13438–13456, https://doi.org/10.1007/s10853-020-04963-2.
69. Elyasi, M.; Derazkola, H.A. Experimental and thermomechanical study on FSW of PMMA polymer T-joint. *Int. J. Adv. Manuf. Technol.* **2018**, https://doi.org/10.1007/s00170-018-1847-7.
70. Hassanifard, S.; Nabavi-Kivi, A.; Ghiasvand, A.; Varvani-Farahani, A. Monotonic and Fatigue Response of Heat-Treated Friction Stir Welded Al 6061-T6 Joints: Testing and Characterization. *Mater. Perform. Charact.* **2021**, *10*, 353–369, https://doi.org/10.1520/MPC20200076.
71. Fu, R.; Zhang, J.; Li, Y.; Kang, J.; Liu, H.; Zhang, F. Effect of welding heat input and post-welding natural aging on hardness of stir zone for friction stir-welded 2024-T3 aluminum alloy thin-sheet. *Mater. Sci. Eng. A* **2013**, *559*, 319–324, https://doi.org/10.1016/j.msea.2012.08.105.